Magnetic Compton profiles of iron and nickel

Y. Kubo
Department of Physics, Colleges of Humanities and Sciences, Nihon University, Tokyo 156, Japan

S. Asano
Institute of Physics, College of Arts and Sciences, The University of Tokyo, Tokyo 153, Japan
(Received 30 March 1990)

Magnetic Compton profiles (MCP's) are calculated for iron and nickel by the full-potential linearized augmented-plane-wave (FLAPW) method on the basis of the local-spin-density approximation. These results are in good agreement with the experimental data of Sakai *et al.* with excellent statistical accuracy. The FLAPW calculations leave slight but noticeable discrepancies in the MCP's along the ⟨100⟩ and ⟨110⟩ directions for iron and the ⟨100⟩ direction for nickel. In the case of iron, the parametrized FLAPW calculations are performed by lowering the center of gravity of p states to reasonably describe the N-centered hole pocket of the minority-spin third band. The MCP's obtained from the parametrized FLAPW calculation show excellent agreement with the experimental data. The comparison of the experimental MCP's of iron and nickel of Sakai *et al.* with the present calculations and others so far reported clearly demonstrates that the MCP investigations are useful for a critical test of the spin-polarized wave functions in the band calculations.

I. INTRODUCTION

Ferromagnetism of iron and nickel is one of the most interesting properties of solids. A substantial number of band-structure calculations[1-9] have been made for iron and nickel. The density-functional theory within the local-spin-density approximation (LSDA)[4] has provided considerable success in describing the electronic properties of these solids, particularly in the magnetic moment. However, in the early magnetic Compton scattering experiment[10-11] of iron, very noticeable discrepancies have been observed in the comparison between the experimental magnetic Compton profiles (MCP's) of polycrystalline iron and the band-theoretical MCP's,[2,12,13] particularly in a low-momentum region (<1 a.u.). This discrepancy has been interpreted as an underestimation of the negatively polarized s-p band electrons. Recently, Cooper *et al.*[14] measured the MCP's of a single crystal of iron using circularly polarized synchrotron-radiation x rays in the three directions ⟨100⟩, ⟨110⟩, and ⟨111⟩, and noticeable anisotropy of the MCP's has been found. Although band-theoretical MCP calculations so far reported[12,13,15] have reasonably reproduced the anisotropy, they have not been successful in quantitatively reproducing the directional MCP's, particularly in the ⟨100⟩ direction.

Very recently, Sakai *et al.*[16] measured the MCP's of a single crystal of iron using circularly polarized 60-keV x rays emitted from an elliptical multipole wiggler installed at the 6.5-GeV storage ring of National Laboratory for High Energy Physics[17] with much higher statistical accuracy compared with the experiments[10-11,14] so far reported. The MCP's by Sakai *et al.*[16] have been consistent with those by Cooper *et al.*[14] within their statistical accuracy. Furthermore, they have also measured the MCP's of a single crystal of nickel by the same technique. The statistical accuracy of the MCP's of nickel is not so high as that of iron, because of the small magnetic moment of nickel, however, the clear anisotropy of the MCP's has been found in a low-momentum region (<1 a.u.). The experimental results of Sakai *et al.*[16] have been compared with our band-theoretical calculations based on the full-potential linearized augmented-plane-wave (FLAPW) method.[18] As a result, good agreement between the theoretical and experimental results have been found for iron and nickel, respectively.

In this paper, the details of the band-theoretical calculations are shown. In the case of iron, standard band calculations[1,2,4] based on the density-functional theory predict the existence of a large minority hole pocket at point N at the Brillouin zone in contrast to the experiments.[19] Therefore, the parametrized FLAPW calculations have been performed by lowering the center of gravity of p states to reasonably reproduce the experimental data, as far as the Fermi-surface topology is concerned. This prescription has been used by Genoud and Singh[15] in the MCP calculations using the linear muffin-tin orbital (LMTO) method. To make clear the origin of the previous discrepancy[10-12,14] between experiment and theory in the MCP's of iron, attempts for discriminating between different calculations are performed, that is, for FLAPW, linearized augmented-plane-wave (LAPW), augmented-plane-wave (APW) calculations, based on the LSDA, and previous calculations.[12,13,15]

The plan of the present paper is as follows. In Sec. II, the procedures of the MCP calculations are provided. In Sec. III, the results are shown and compared with the experiments by Sakai *et al.*[16] In Sec. IV, the adequacy of the band theory based on the LSDA for describing the MCP's of iron and nickel is discussed through the comparison of the experimental data of Sakai *et al.*[16] with

the present calculations and other ones. The conclusions are presented in Sec. V.

II. CALCULATION PROCEDURE

The FLAPW method based on the LSDA is employed to calculate the energy band structures and the wave functions in iron and nickel. The energy values and wave functions of iron and nickel are calculated at 55 and 89 **k** points, respectively, in $\frac{1}{48}$ of the Brillouin zone for each spin state. The exchange-correlation functional form given by von Barth and Hedin[20] is used. The LAPW method[21] in a scalar relativistic version is employed, and the charge density as well as the potential is expanded into a spherical harmonics inside the inscribed sphere of radii RI and in a Fourier series for the interstitial region. In these expansions, the crystal symmetry is taken into account. The inscribed spheres can be chosen more or less arbitrarily, and in the present calculations the RI's of iron and nickel are kept at 2.270 39 a.u. and 2.258 96 a.u., respectively. The lattice constants for iron and nickel are assigned to be 5.4057 a.u. and 6.6440 a.u. respectively. The spherical harmonics (Y_{LM}) expansions of the charge density and the potential are truncated at $L=8$, and about 100 plane waves are used as basis functions. In the case of iron, parametrized FLAPW band-structure calculations are performed by lowering the center of gravity of p states to reproduce a reasonable description of the Fermi-surface topology[19] (in particular the minority N-centered hole pocket).

From the energy values and wave functions thus obtained, the spin- (σ) dependent momentum density distributions (SMDD's) $\rho_b^\sigma(p)$'s by band electrons in iron and nickel are determined for 1253 and 893 reciprocal lattice vectors, which include more than 99% of the total number of band electrons, respectively. The SMDD's $\rho_c^\sigma(p)$'s contributed by the core electrons are evaluated from free-atom wave functions obtained by using the von Barth–Hedin exchange-correlation potential based on the LSDA for iron and nickel, respectively. From the respective $\rho_{b,c}^+(p)$'s and $\rho_{b,c}^-(p)$'s for the majority (+) and minority (−) spin states in iron and nickel, the magnetic Compton profiles $J_{\rm mag}^b(p_z)$'s and $J_{\rm mag}^c(p_z)$'s are calculated for the band and core electrons, respectively

$$J_{\rm mag}^{b,c}(p_z)=\int[\rho_{b,c}^+(p)-\rho_{b,c}^-(p)]dp_x dp_y \ .$$

The theoretical magnetic Compton profiles $J_{\rm mag}(p_z)$'s for iron and nickel are obtained by adding $J_{\rm mag}^b(p_z)$'s and $J_{\rm mag}^c(p_z)$'s, respectively. In the comparison of the theoretical $J_{\rm mag}(p_z)$'s with the experiments by Sakai *et al.*[16], convoluted results with the experimental resolution[16] [a Gaussian function with full width at half maximum (FWHM) 1.0 a.u.] are used.

III. RESULTS

A. Calculated results

1. Iron

The band structure calculated by the parametrized FLAPW method is shown in Fig. 1. It is in good general agreement with other parametrized band structures.[22]

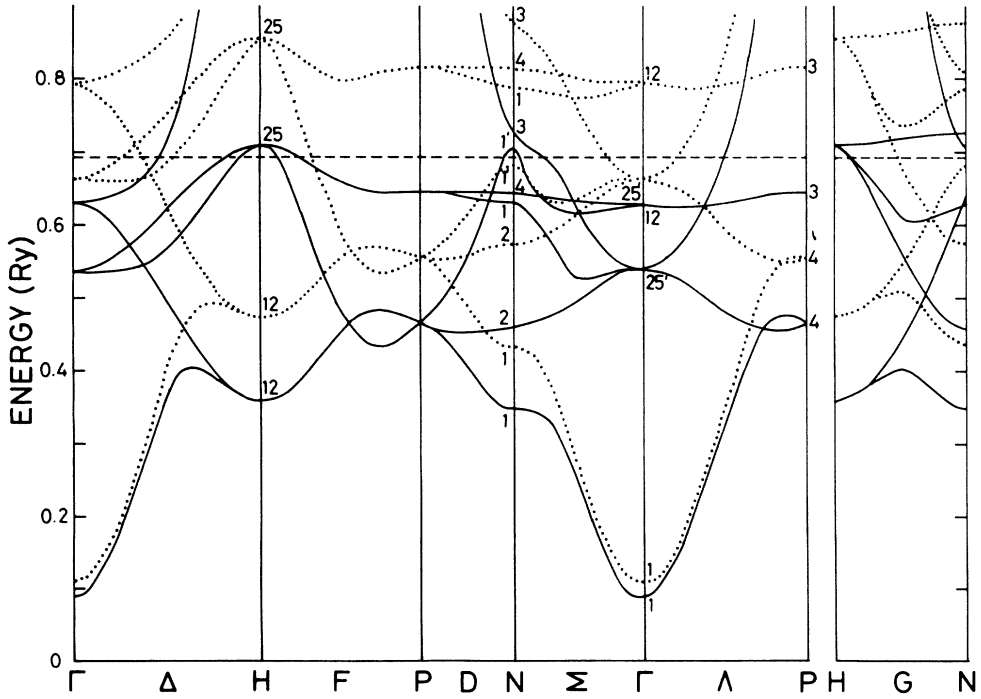

FIG. 1. Energy-band structure of ferromagnetic iron. Majority spin states are denoted by a solid line, minority spins by a dotted line. The dashed line shows the Fermi level.

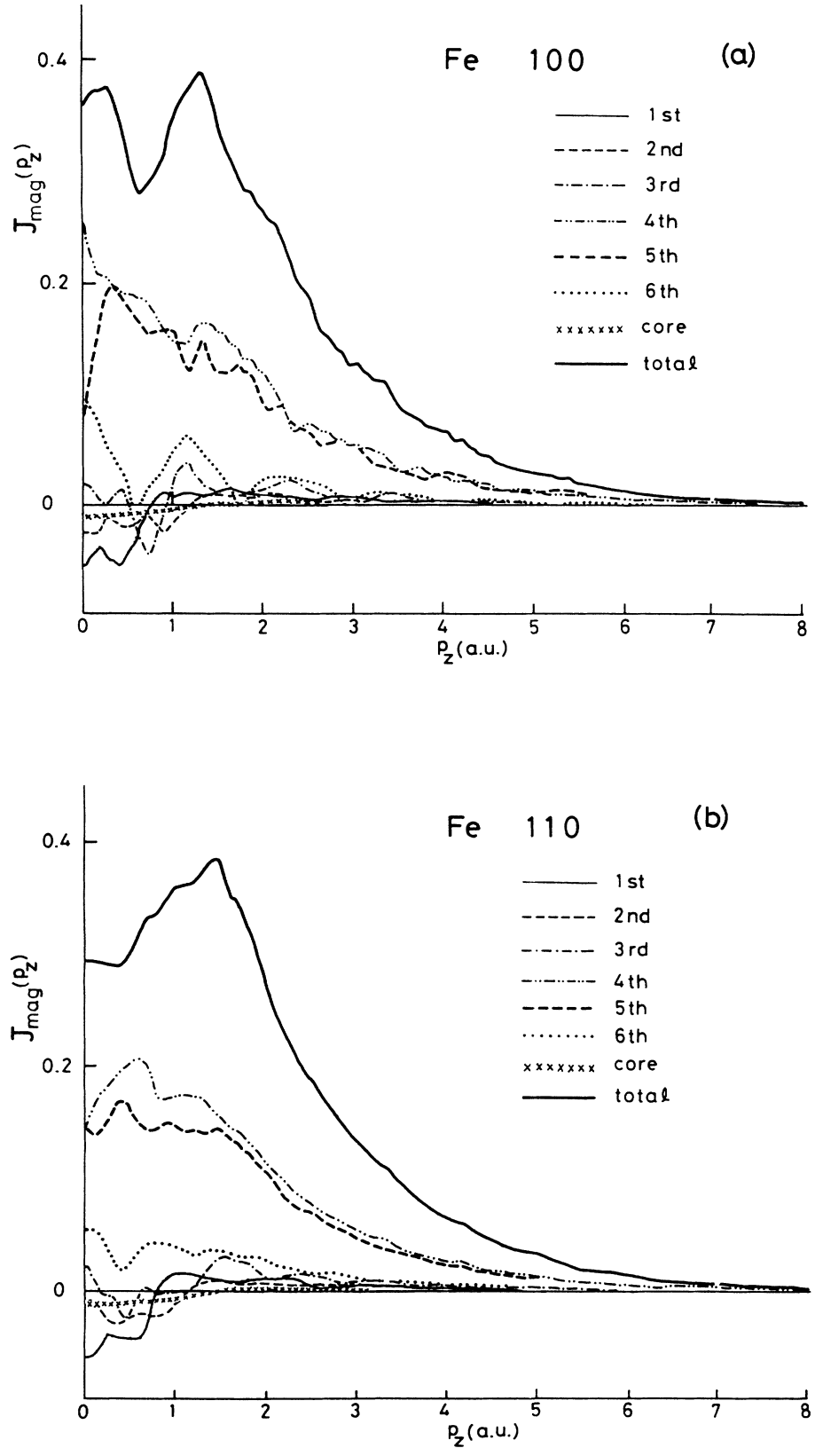

FIG. 2. Theoretical magnetic Compton profiles (MCP's) of iron calculated by the parametrized FLAPW method, for (a) ⟨100⟩, (b) ⟨110⟩, and (c) ⟨111⟩ directions. The bold solid lines show the total MCP's. The partial contributions to the MCP's from each band (from the first to the sixth band) and core electrons are also shown.

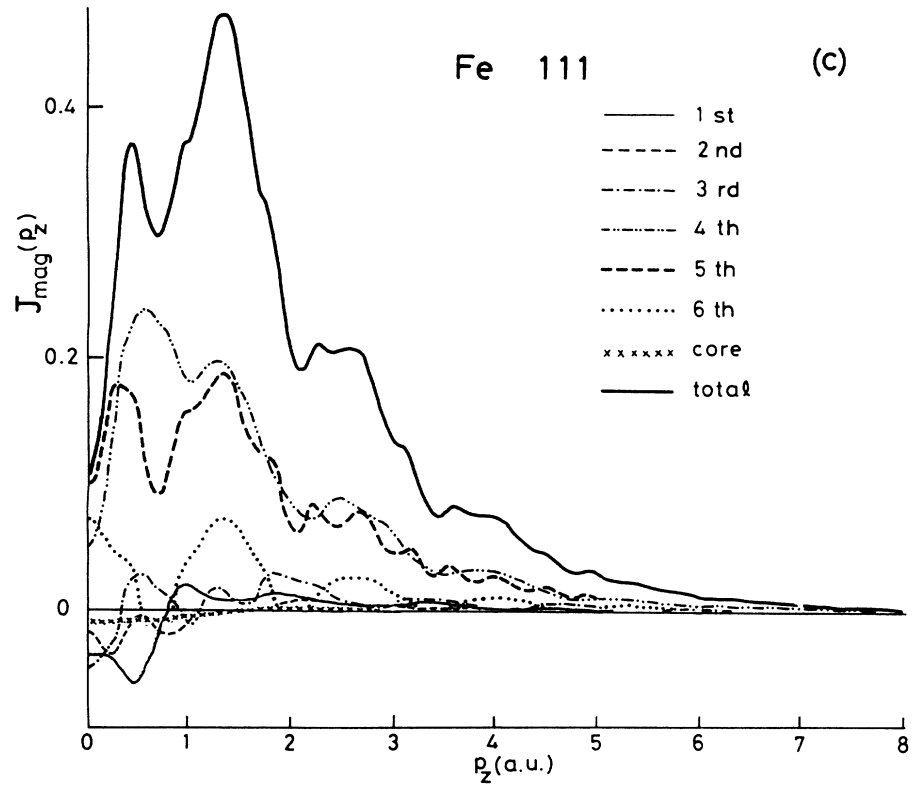

FIG. 2. (*Continued*).

The important result introduced by the parametrized band structure is the disappearance of the N-centered hole pocket in the third minority-spin band. Other points of the Brillouin zone are not so drastically affected. The exchange splitting varies substantially over the d band as seen from Fig. 1, ranging from 1.5 eV near the bottom of the band to 2.2 eV near the top. The exchange splitting of predominantly s-like states (Γ_1) is about 0.3 eV, and that of p-like states (N_1') is about -0.3 eV due to lowering the center of gravity of p states. Although a precise experimental value for a typical exchange splitting directly compared with band-structure calculations is not known, the exchange splitting determined by photoemission experiments[23] is referred to here. The exchange splitting (Δ_{exc}) of d bands has been determined at the symmetric points Γ, P, H, and N: Δ_{exc} at Γ_{25}' [$\Delta_{exc}(\Gamma_{25}')$] is 2.08 ± 0.10 eV, Δ_{exc} $(P_4)=1.35\pm0.10$ eV, $\Delta_{exc}(H_{12})$ $=1.30\pm0.30$ eV, and $\Delta_{exc}(N_2)=1.60\pm0.15$ eV. The corresponding calculated values are $\Delta_{exc}(\Gamma_{25}')=1.72$ eV, $\Delta_{exc}(P_4)=1.21$ eV, $\Delta_{exc}(H_{12})=1.54$, and $\Delta_{exc}(N_2)=1.55$ eV. The calculated magneton number $2.07\mu_B$ is slightly smaller than the experimental value[24] $2.12\mu_B$. The negatively polarized contribution, that is, both the negative polarization of the s-p electrons and the electrons outside the inscribed sphere, is $-0.135\mu_B$, and the value is a figure of about half the neutron data.[25]

The theoretical $J_{mag}(p_z)$'s in the three directions $\langle 100\rangle$, $\langle 110\rangle$, and $\langle 111\rangle$ are shown by bold solid lines in Fig. 2. General features of the $J_{mag}(p_z)$'s in the figure are as follows: In low-momentum region $p_z<2$ a.u., characteristic structures are observed. That is, in the $\langle 100\rangle$ direction, bulges around 0.2 and 1.3 a.u., and a depression around 0.6 a.u. are observed. In the $\langle 110\rangle$ direction, a central depression with a flat bottom and an overall bulge around 1.5 a.u. are observed. In the $\langle 111\rangle$ direction, a sharp central dip, a peak near 0.4 a.u., and a bulge with a peak near 1.3 a.u. are observed. In the high-momentum region $p_z>2$ a.u., structureless similar shapes are observed for the $\langle 100\rangle$ and $\langle 110\rangle$ directions.

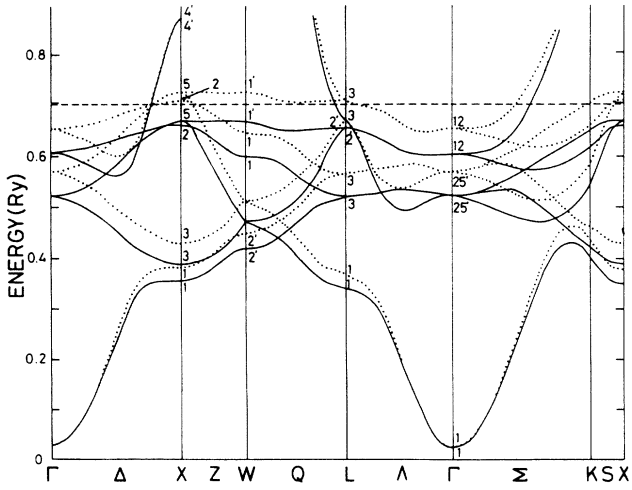

FIG. 3. Energy-band structure of ferromagnetic nickel. Majority-spin states are denoted by a solid line; minority spins by a dotted line. Dashed line shows the Fermi level.

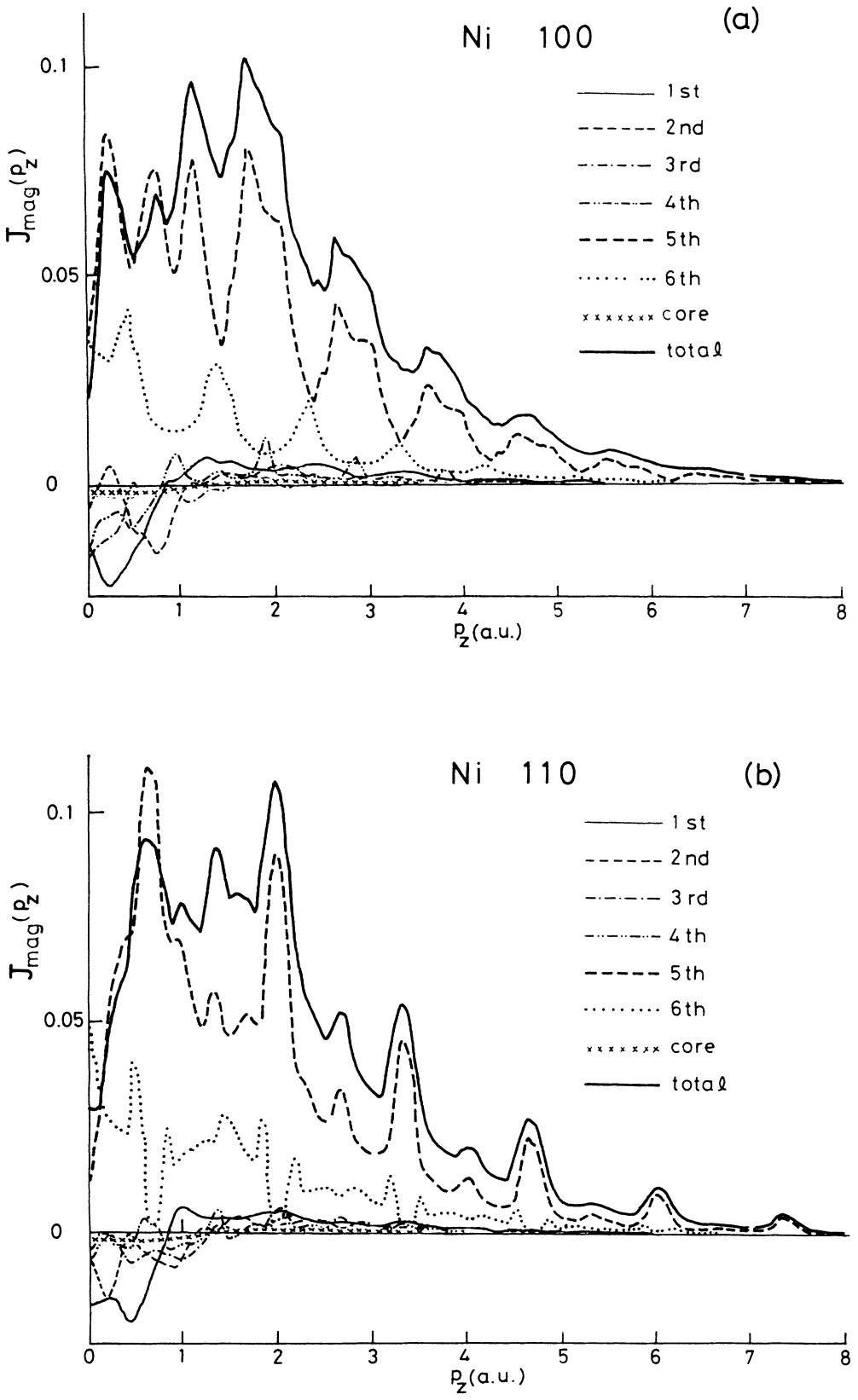

FIG. 4. Theoretical magnetic Compton profiles (MCP's) of nickel calculated by the FLAPW method, for (a) ⟨100⟩, (b) ⟨110⟩, and (c) ⟨111⟩ directions. The bold solid lines show the total MCP's. The partial contributions to the MCP's from each band (from the first to the sixth band) and core electrons are also shown.

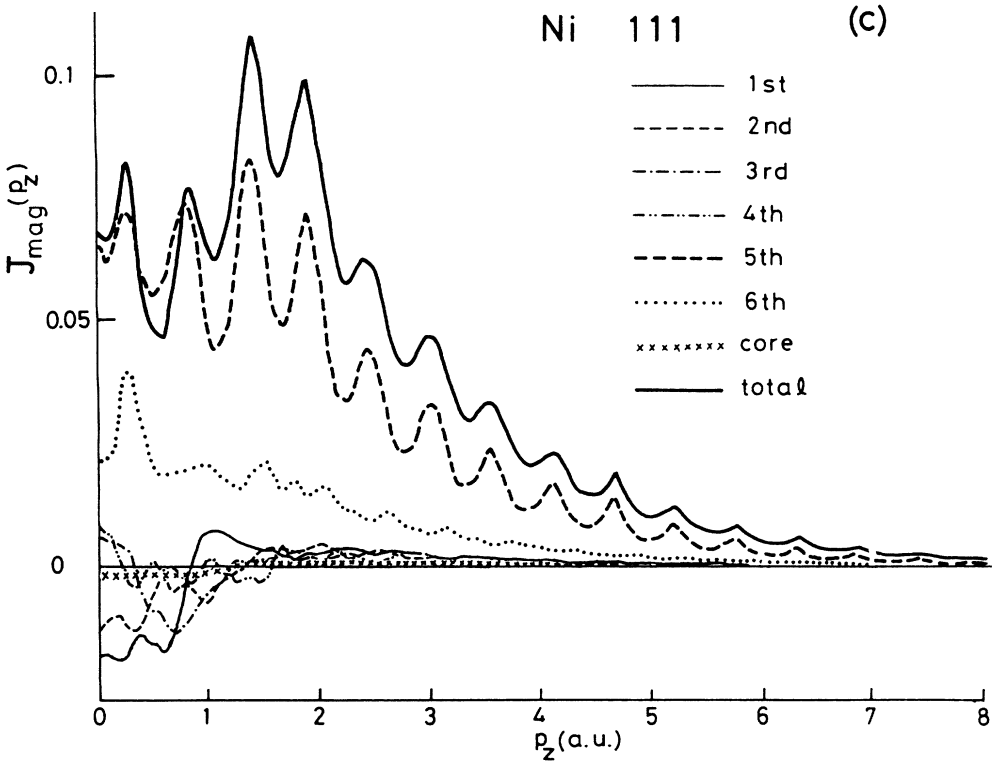

FIG. 4. (*Continued*).

However, noticeable structures are observed in the region $2 < p_z < 5$ a.u. for the $\langle 111 \rangle$ direction. In order to see the origin of the structures, partial $J_{mag}(p_z)$'s from each electron state are also shown in Fig. 2. Isotropic negative contributions to the $J_{mag}(p_z)$ from the first band are observed in the three directions $\langle 100 \rangle$, $\langle 110 \rangle$, and $\langle 111 \rangle$ at $p_z < 1$ a.u., and these are mainly due to negative polarization of *s*-like electrons as expected from the band structure in Fig. 1. On the other hand, negative contributions from the second and third bands at $p_z < 1$ a.u. are mainly due to negative polarization of *p*-like electrons. The contributions from the fourth, fifth, and sixth bands are positive in all momentum regions, and have strong directional dependence at $p_z < 1$ a.u. The characteristic structures at $p_z < 1$ a.u. from the fourth to the sixth bands are attributed to both the anisotropic *d*-like electron distributions and the Fermi-surface topology.

2. Nickel

The band structure by the FLAPW method is shown in Fig. 3. It is in good overall correspondence with other band structures.[3-5] The exchange splitting varies over the *d* band, ranging from 0.55 eV near the bottom of the band to 0.76 eV near the top, as seen from Fig. 3. The exchange splitting of predominantly *s* and *p* states (Γ_1, L_2, and X_4) is about 0.02 eV. The magnitude of the exchange splitting throughout the *d* band determined by the photoemission experiments[26-28] differs roughly by a factor of 2 from the calculated values. However, it should be noted that photoemission experiments measure the excitation spectrum of a solid, whereas in band calculations the ground-state eigenvalue spectrum is determined.[29] The calculated magneton number $0.58\mu_B$ is slightly larger than the experimental value[24] $0.56\mu_B$. The negatively polarized contribution from the *s*-*p* electrons and the electrons outside the inscribed sphere is $-0.047\mu_B$.

The calculated $J_{mag}(p_z)$'s in the three directions $\langle 100 \rangle$, $\langle 110 \rangle$, and $\langle 111 \rangle$ are shown by bold solid lines in Fig. 4. It is noted that the scales of the $J_{mag}(p_z)$'s in nickel are about four times larger than those in iron. The characteristic directional differences of the $J_{mag}(p_z)$'s are observed in the figure. That is, in the $\langle 100 \rangle$ direction, a sharp central dip, peaks near 0.2 and 0.7 a.u., and umklapp images[30] in $p_z > 1$ a.u. are observed. In the $\langle 110 \rangle$ direction, a deep central dip, a peak around 0.6 a.u., and umklapp images $p_z > 1$ a.u. are noticed. In the $\langle 111 \rangle$ direction, peaks near 0.2 and 0.8 a.u., and umklapp images in $p_z > 1$ a.u. appear. In order to see the origins of these features, partial $J_{mag}(p_z)$'s from each electron state are also shown in Fig. 4. The partial contributions from the first band are negative and isotropic in $p_z < 1$ a.u., and these are mainly due to the negative polarization of *s*-like electrons as expected from the band structure in Fig. 3. The negative contribution from the second to fourth bands in $p_z < 1$ a.u. are mainly attributed to the negative polarization of *p*-like electrons. The partial contributions from the fifth and sixth bands are positive and provide noticeable structures with umklapp processes, and those from the fifth band construct the main structures of the $J_{mag}(p_z)$'s. These characteristic structures from the fifth

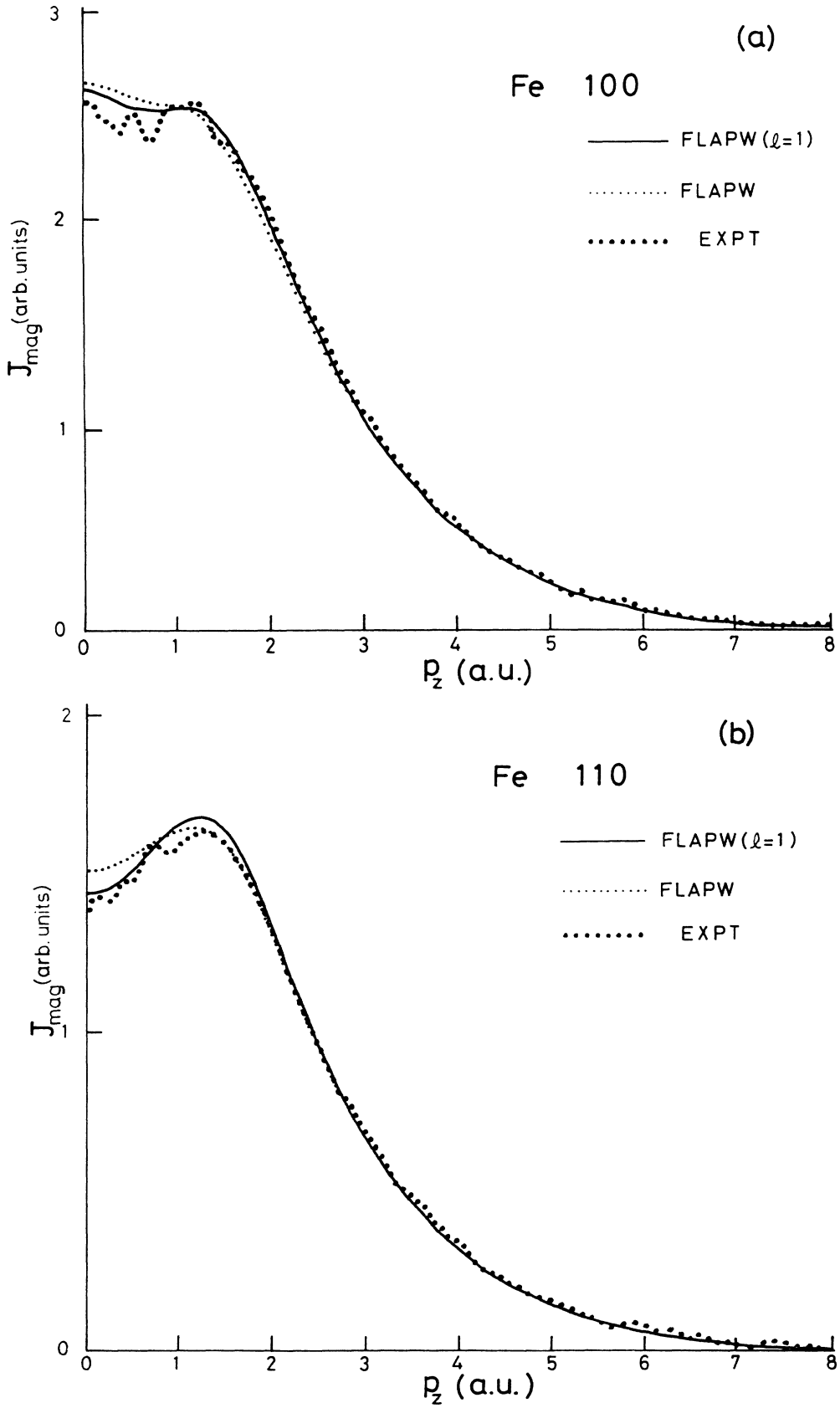

FIG. 5. Magnetic Compton profiles (MCP's) of iron for (a) ⟨100⟩, (b) ⟨110⟩, and (c) ⟨111⟩ directions. The bold solid and thin dotted lines show the theoretical MCP's calculated by the parametrized FLAPW and FLAPW methods, respectively. These are convoluted with a Gaussian function having FWHM 1.0 a.u. The bold dotted lines represent the linear interpolated experimental results (Ref. 16). The area of each theoretical profile is normalized to the corresponding experimental one.

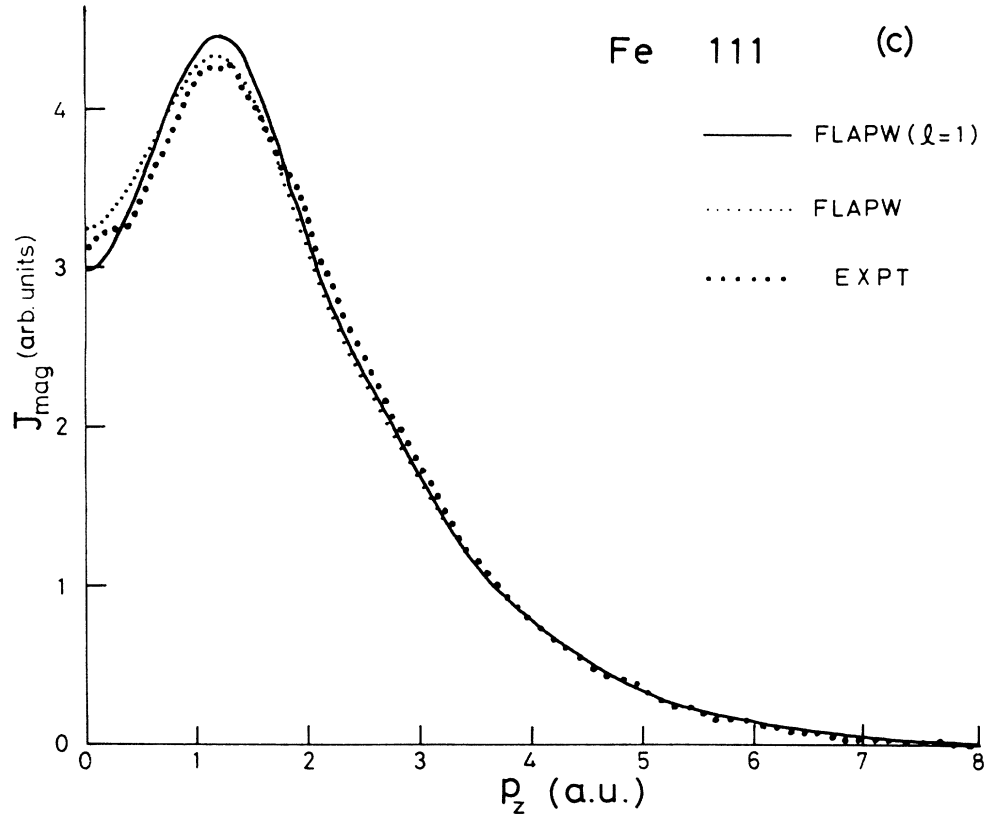

FIG. 5. (*Continued*).

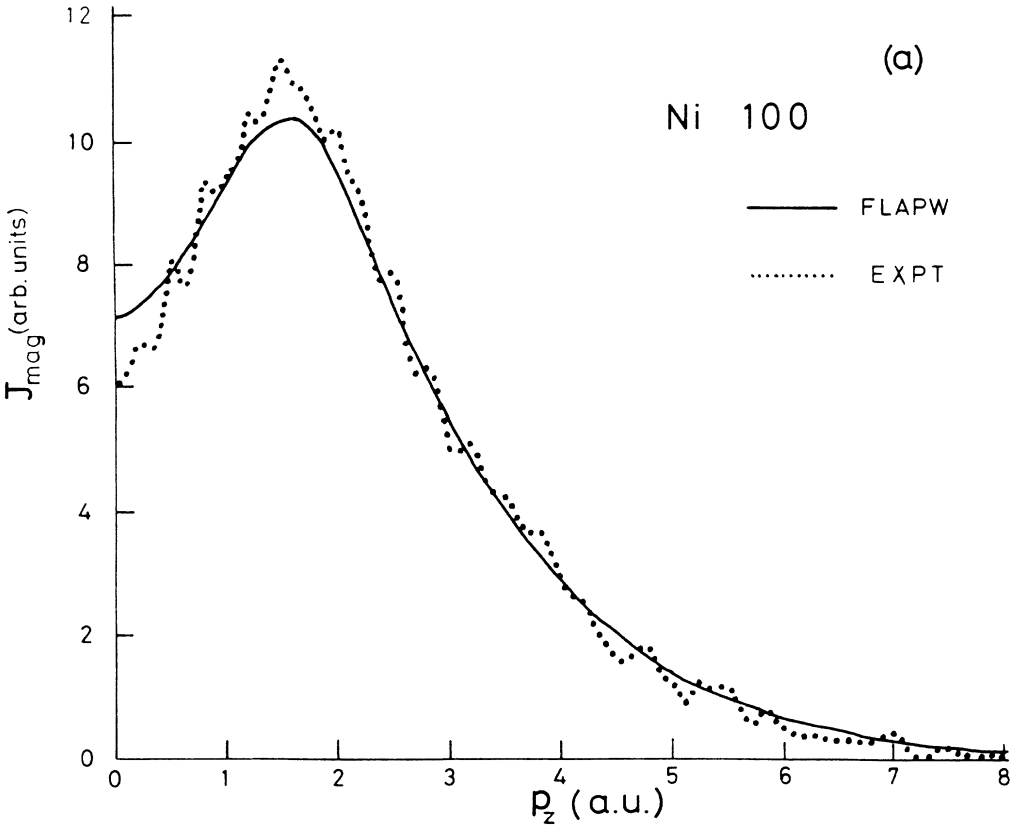

FIG. 6. Magnetic Compton profiles (MCP's) of nickel for (a) ⟨100⟩, (b) ⟨110⟩, and (c) ⟨111⟩ directions. The bold solid lines show the theoretical MCP's calculated by the FLAPW method. These MCP's are convoluted with a Gaussian function having FWHM 1.0 a.u. The bold dotted lines represent linear interpolated experimental results (Ref. 16). The area of each theoretical profile is normalized to the corresponding experimental one.

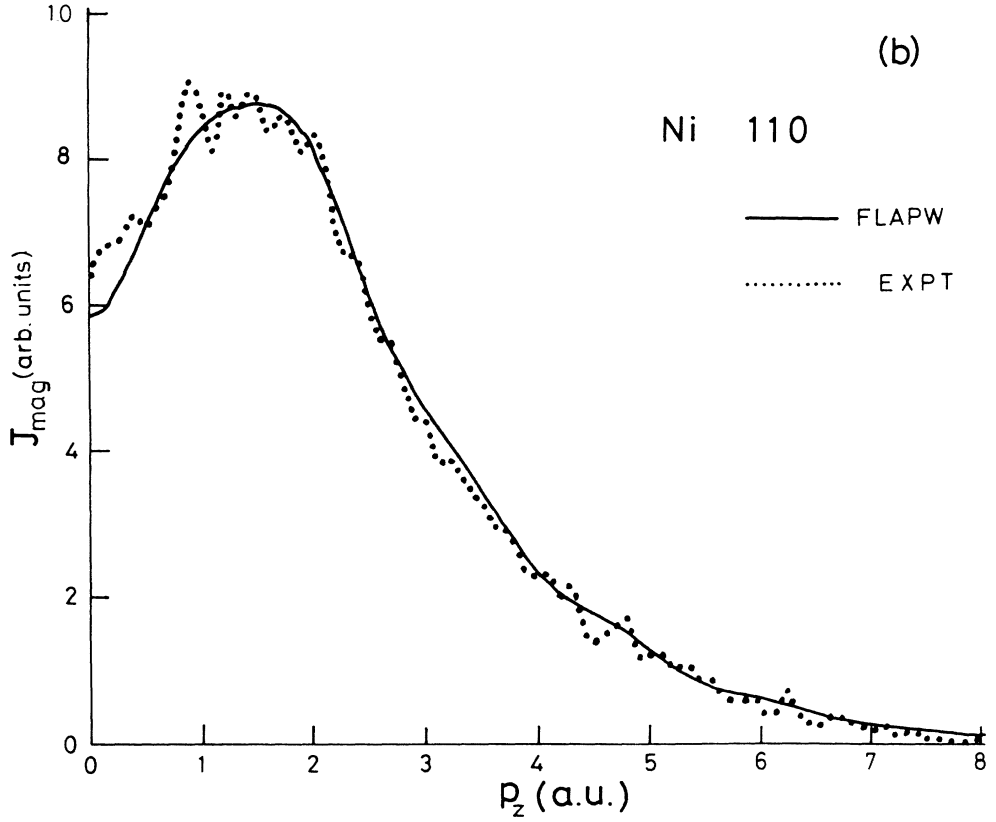

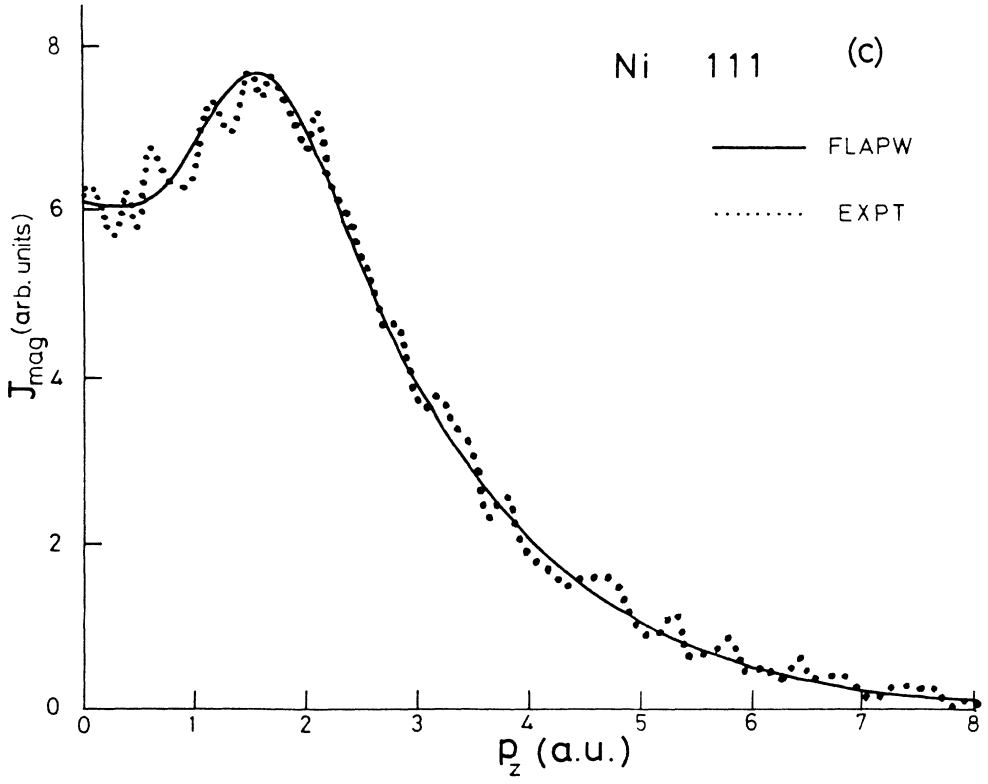

FIG. 6. (*Continued*).

to the sixth bands are dominantly due to both anisotropic d-like electron distributions and the Fermi-surface topology.

B. Comparison with experiment

1. Iron

The experimental directional $J_{\rm mag}(p_z)$'s of Sakai *et al.*[16] are shown by bold dots in Fig. 5. Our convoluted results with FWHM 1.0 a.u. are also shown by solid curves in the figure. As seen from the figure, the agreement between the theoretical and experimental results is excellent. The previous significant discrepancy[14] between theory and experiment in the $J_{\rm mag}(p_z)$ along the $\langle 100 \rangle$ direction is not observed in Fig. 5.

2. Nickel

In Fig. 6, experimental $J_{\rm mag}(p_z)$'s of Sakai *et al.*[16] are shown by bold dots, and our convoluted results with FWHM 1.0 a.u. are also given by solid curves. The agreement between theory and experiment is also good, particularly in the $J_{\rm mag}(p_z)$ along the $\langle 111 \rangle$ direction. The statistical accuracy of the experimental $J_{\rm mag}(p_z)$ of nickel is not so high as that of iron,[16] because of the small magnetic moment of nickel. However, a slight disagreement between the theoretical and experimental results is observed, particularly on the hollow around the origin of the $\langle 100 \rangle$ $J_{\rm mag}(p_z)$.

IV. DISCUSSIONS

As seen in the preceding section, the directional $J_{\rm mag}(p_z)$'s of iron calculated by the parametrized FLAPW method are in excellent agreement with those measured by Sakai *et al.*[16] with high statistical accuracy. The good agreement between the FLAPW calculations and the experiments[16] is also found in the $J_{\rm mag}(p_z)$ of nickel. Most measurements of $J_{\rm mag}(p_z)$'s so far reported have been done on iron, and in the previous comparison between the experimental data[10,11,14] and the band-theoretical predictions,[2,12,13,15] a good agreement has not been found. In order to make clear the origin of the previous disagreement, the accuracy of the band model based on the LSDA in describing the $J_{\rm mag}(p_z)$'s of iron and nickel is investigated.

First, the effect on the $J_{\rm mag}(p_z)$ of iron due to lowering the center of gravity of p states described in Sec. II (parametrization in FLAPW calculation), which leads mainly to the increase of a negative polarization of p electrons, is examined. Therefore, the FLAPW calculation of the $J_{\rm mag}(p_z)$ of iron is performed using the same procedure except the parametrization as mentioned in Sec. II. The magneton number calculated by the FLAPW method is $2.08\mu_B$. The $J_{\rm mag}(p_z)$'s by the FLAPW calculations are compared with those by the parametrized FLAPW ones in Fig. 7. As noticed from the figure, the $J_{\rm mag}(p_z)$'s of the parametrized FLAPW calculations are lower in $p_z < 1$ a.u. and higher in $1 < p_z < 2$ a.u. than those from the FLAPW ones. In order to see this trend clearly, the convoluted FLAPW calculations with a Gaussian of FWHM 1.0 a.u. are also shown in Fig. 5. As seen from the trend observed in the figure, the parametrization effect is useful, that is, the parametrized FLAPW calculations are closer to the experiments than the FLAPW ones. However, it is noted that the parametrization effect is not so large as Genoud and Singh[15] have indicated in the LMTO calculations. Second, non-muffin-tin (NMT) effects on the $J_{\rm mag}(p_z)$'s of iron are examined. Then, the $J_{\rm mag}(p_z)$'s are calculated by the LAPW method with a muffin-tin (MT) potential. The calculations are performed using the procedure in Sec. II except the parametrization and NMT potential parts. The magneton number calculated by the LAPW method is $2.22\mu_B$. The calculated $J_{\rm mag}(p_z)$'s are compared with those by the FLAPW method in Fig. 7. The $J_{\rm mag}(p_z)$'s by the LAPW method are generally higher than those by the FLAPW method because of the larger magneton number. In the comparison between the normalized results to the experiments by Sakai *et al.*,[16] the FLAPW calculations are closer to the experiments than the LAPW ones, however, the differences are small. Third, in order to test the accuracy of the LAPW calculations of the $J_{\rm mag}(p_z)$'s of iron, the comparison between the LAPW and APW calculations is performed. The APW calculations are carried out using a MT potential by the procedure mentioned in Sec. II except the parametrization and NMT potential parts. The magneton number obtained by the APW calculation is $2.22\mu_B$. The $J_{\rm mag}(p_z)$'s by the APW calculations are shown in Fig. 7. It is noticed from the figure that the APW calculations are quite similar to those by the LAPW ones. This confirms the capability of the LAPW method to describe the $J_{\rm mag}(p_z)$ of iron. Fourth, the contribution to the $J_{mag}(p_z)$'s of iron due to the scalar-relativistic (SR) effect is examined through the comparison between the LAPW calculations with and without the SR effect. As a result, it is found that the SR effect on the $J_{\rm mag}(p_z)$'s of iron is negligibly small. The effect of spin-obit interactions on the $J_{\rm mag}(p_z)$ of iron has not been examined. Although this effect should be taken into account in the investigation of magnetotransport experiments,[31] the contribution to the $J_{\rm mag}(p_z)$ of iron may be in a smaller extent.

On the other hand, in the case of nickel, the examination performed in iron except for the first has also been carried out, and similar results to those found in iron have also been obtained. The FLAPW calculations in nickel leave the slight but noticeable discrepancy in the $J_{\rm mag}(p_z)$ along the $\langle 100 \rangle$ direction. It seems that this discrepancy is attributed to nonlocal potential effects which are not included in the present calculations based on the LSDA. Actually, there exists the problem[8] concerning the existence of a hole pocket associated with the X point in the third minority-spin band. In the present calculations of nickel, nonlocal potential effects on the $J_{\rm mag}(p_z)$ have not been examined, since the contribution to the $J_{\rm mag}(p_z)$ due to spin-orbit interactions should first be investigated, and the statistical accuracy of the experimental[16] $J_{\rm mag}(p_z)$'s is not so high as that of iron.

Next, a comparison between the present and other theoretical calculations of the $J_{\rm mag}(p_z)$'s of iron and nick-

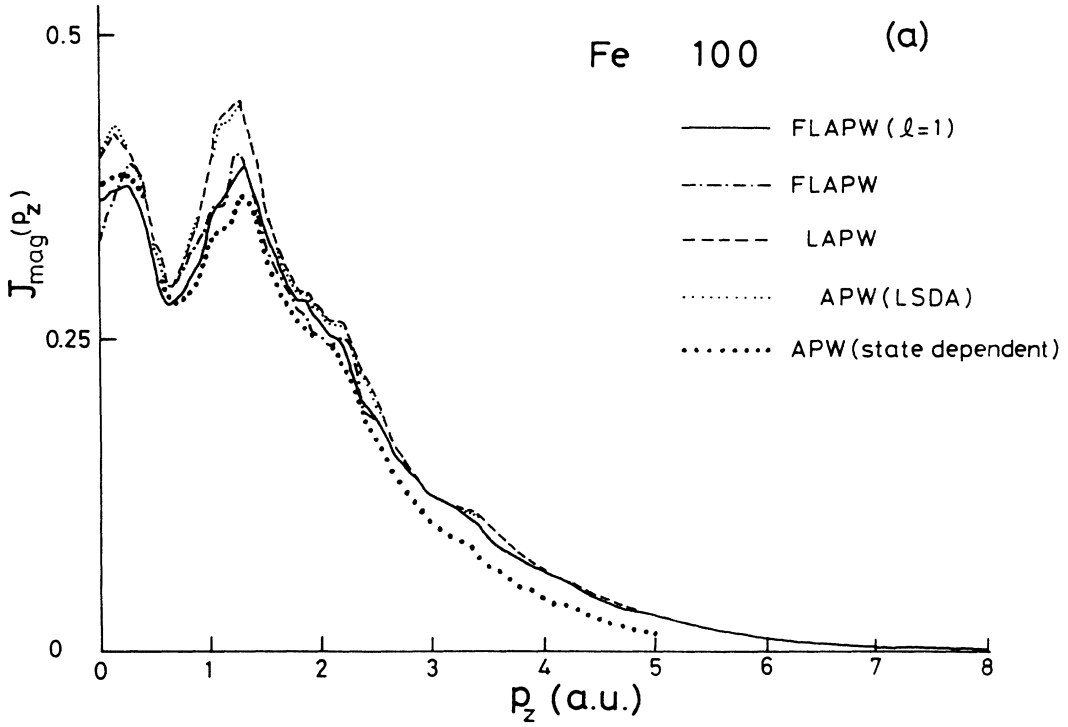

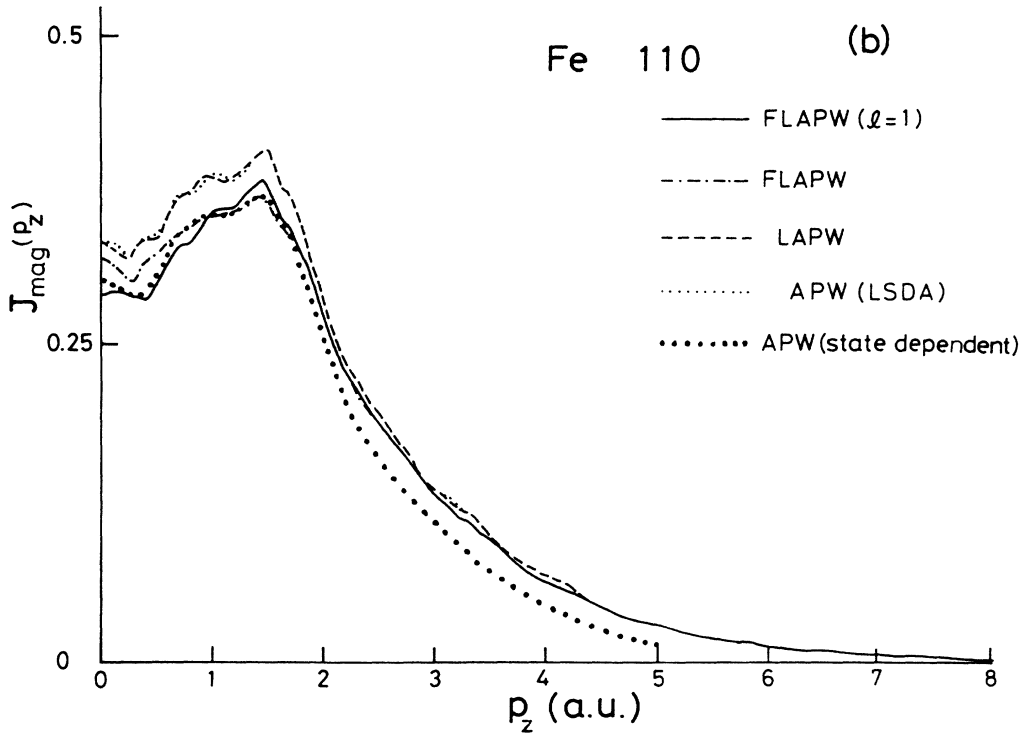

FIG. 7. Theoretical magnetic Compton profiles (MCP's) of iron for (a) ⟨100⟩, (b) ⟨110⟩, and (c) ⟨111⟩ directions. The MCP's represented by FLAPW ($l=1$), FLAPW, LAPW, and APW (LSDA) correspond to present calculations, and the parametrized FLAPW calculation is denoted by FLAPW ($l=1$). The MCP's denoted by APW (state dependent) correspond to previous calculations (Ref. 12).

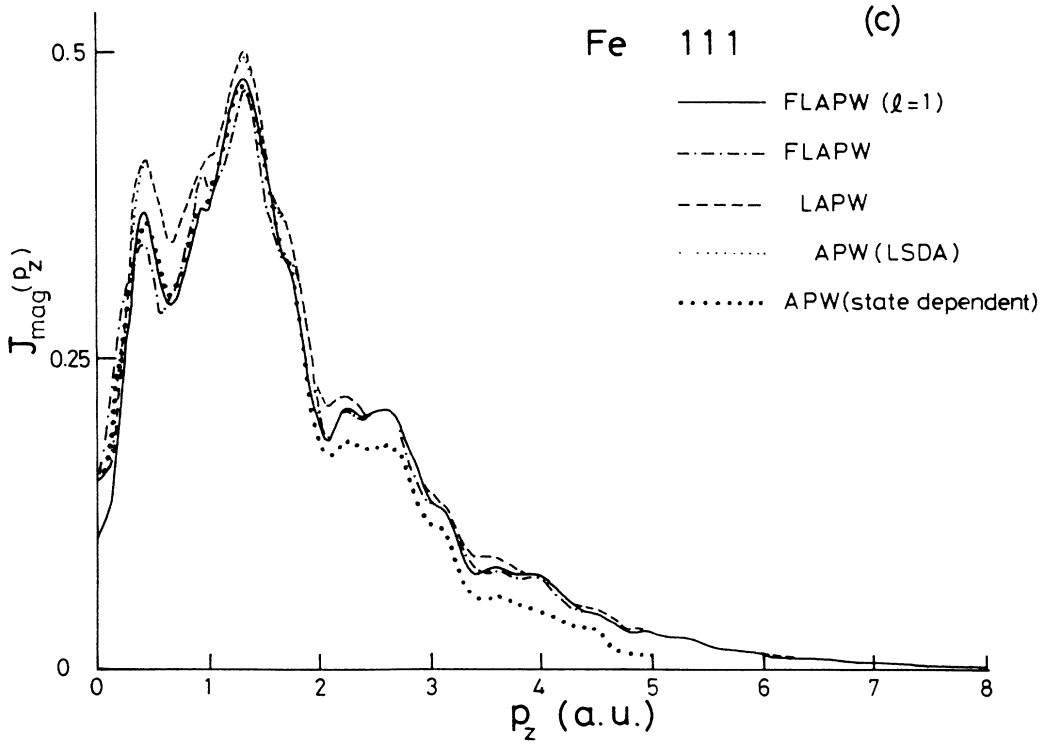

FIG. 7. (*Continued*).

el is performed. First, the present APW calculations of iron are compared with the previous APW ones[12] in Fig. 7. As seen from the figure, the previous APW calculations are generally lower compared with those by the present APW ones, because of the previous calculations of momentum densities limited to $p < 5$ a.u. Overall shapes between both calculations are similar. Now, the previous APW band structure of iron has been calculated by using a state-dependent potential. In the previous APW band structure, the N-centered hole pocket of the third minority-spin band that appears in the present APW calculation, disappeared. Nevertheless, the $J_{\rm mag}(p_z)$'s of the previous APW calculations around $p_z=0$ a.u. are higher than those around $p_z=1.2$ a.u., in the $\langle 100 \rangle$, direction, in contrast to the case of the present APW calculation. Furthermore, the previous APW calculation has been extended to $p < 7.5$ a.u. (Ref. 14). These previous APW calculations have been compared with experiments,[10,11,14] and some discrepancies have been found. Particularly, it has been indicated[14] that the previous APW calculation predicts much higher values at $p_z < 1$ a.u. in the $\langle 100 \rangle$ direction than the experimental result. In order to examine this situation, the extended APW calculations are compared with the present parametrized FLAPW, FLAPW, and LAPW calculations in Fig. 8. Since the $J_{\rm mag}(p_z)$'s of the extended APW calculations[14] have been convoluted with a Gaussian of FWHM 0.7 a.u., the present calculations are also convoluted with a Gaussian of FWHM 0.7 a.u. The extended APW calculations correspond to the magneton number $2.2\mu_B$. As noticed from Fig. 8, the extended APW calculations are clearly higher at $p_z < 1$ a.u. in all directions than the corresponding present calculations. From these results, it may be indicated that the state-dependent potential[12] used in the previous band-structure calculations is inadequate to describe the $J_{\rm mag}(p_z)$'s in iron, probably for representation of the negative spin polarization of p-like electrons. Second, the parametrized FLAPW calculations of iron are compared with the parametrized LMTO ones by Genoud and Singh.[15] The parametrized LMTO band structure of iron has been calculated by lowering the center of gravity of p states to correctly reproduce the Fermi-surface topology, in particular the minority N-centered hole pocket. In the comparison of the $J_{\rm mag}(p_z)$'s of the parametrized LMTO calculations with the experimental data of Cooper *et al.*,[14] it has been found that the calculated $J_{\rm mag}(p_z)$'s are close to the experimental data, particularly in the $\langle 110 \rangle$ and $\langle 111 \rangle$ directions, but the theoretical results are still overestimated near $p_z=0$ a.u., especially in the $\langle 100 \rangle$ direction. The parametrized LMTO calculations,[15] which have been convoluted with a Gaussian of FWHM 0.7 a.u., are compared with different calculations, that is, the present parametrized FLAPW, FLAPW, LAPW calculations, and the previous APW ones, in Fig. 8. The parameterized LMTO $J_{\rm mag}(p_z)$'s, which correspond to the magnetic moment of $2.12\mu_B$ are similar to our results, particularly to the parametrized FLAPW ones. However, as seen from the comparison of these relative values of $J_{\rm mag}(p_z)$'s, the parametrized LMTO results are higher at $p_z < 1$ a.u., especially in the $\langle 100 \rangle$ direction, and lower at $p_z > 5$ a.u. than the parametrized FLAPW ones, respectively. Third, we mention the Korringa-Kohn-Rostoker (KKR) calculations of Poulter and Staunton.[13] Since the

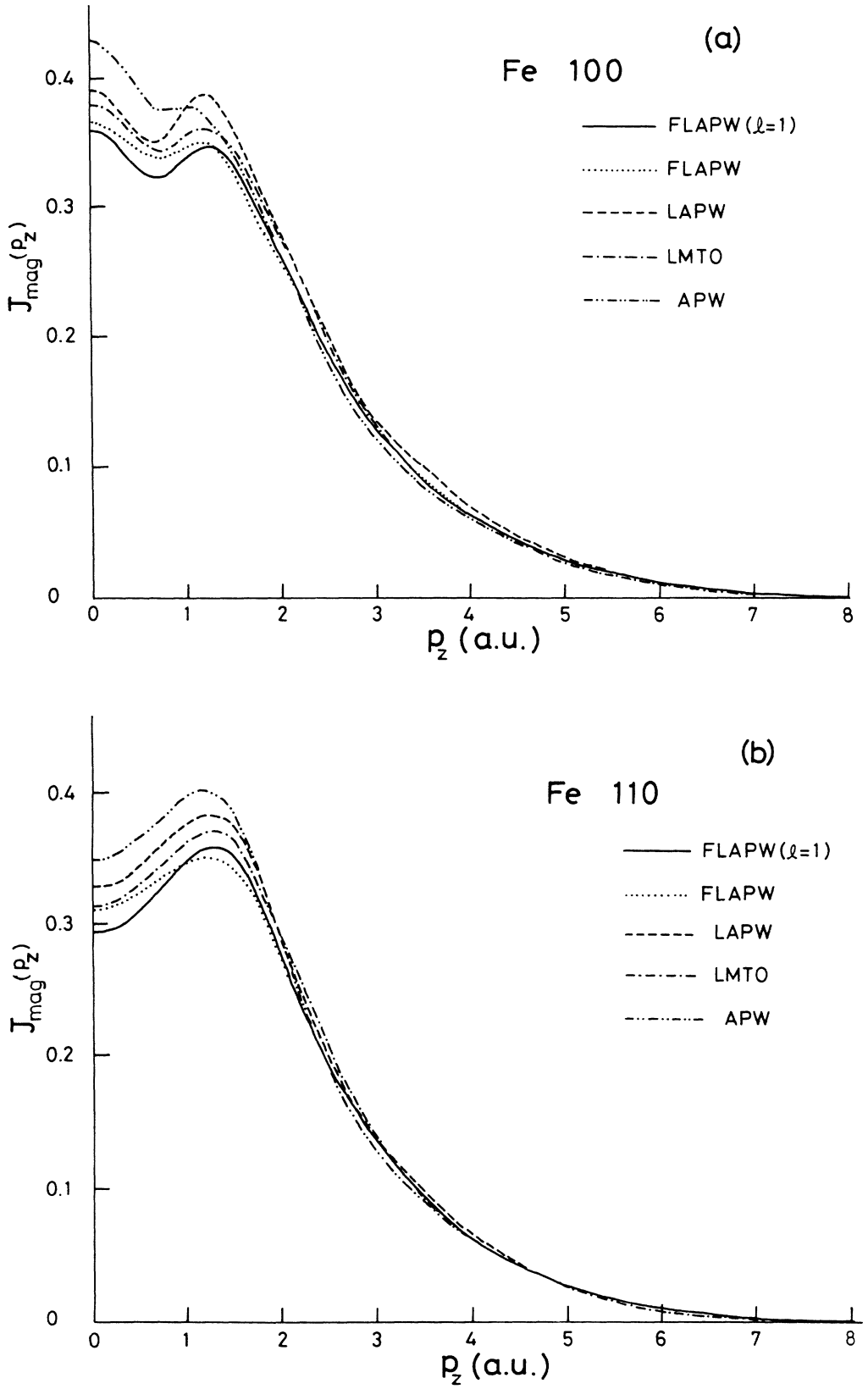

FIG. 8. Theoretical magnetic Compton profiles (MCP's) of iron for (a) ⟨100⟩, (b) ⟨110⟩, and (c) ⟨111⟩ directions. The MCP's denoted by FLAPW ($l=1$), FLAPW, and LAPW correspond to present calculations, and the FLAPW ($l=1$) represents the parametrized FLAPW calculation. The MCP's denoted by LMTO and APW correspond to LMTO calculations (Ref. 15) and APW ones (Ref. 14), respectively. These results are convoluted with a Gaussian function having FWHM 0.7 a.u.

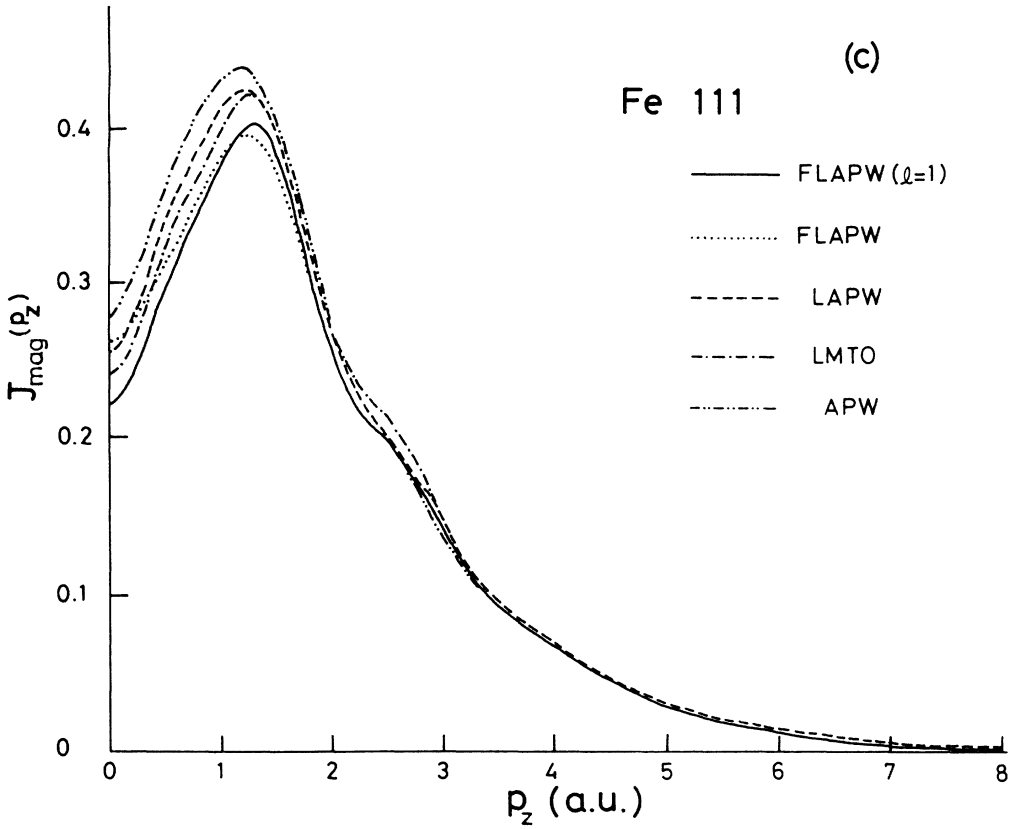

FIG. 8. (*Continued*).

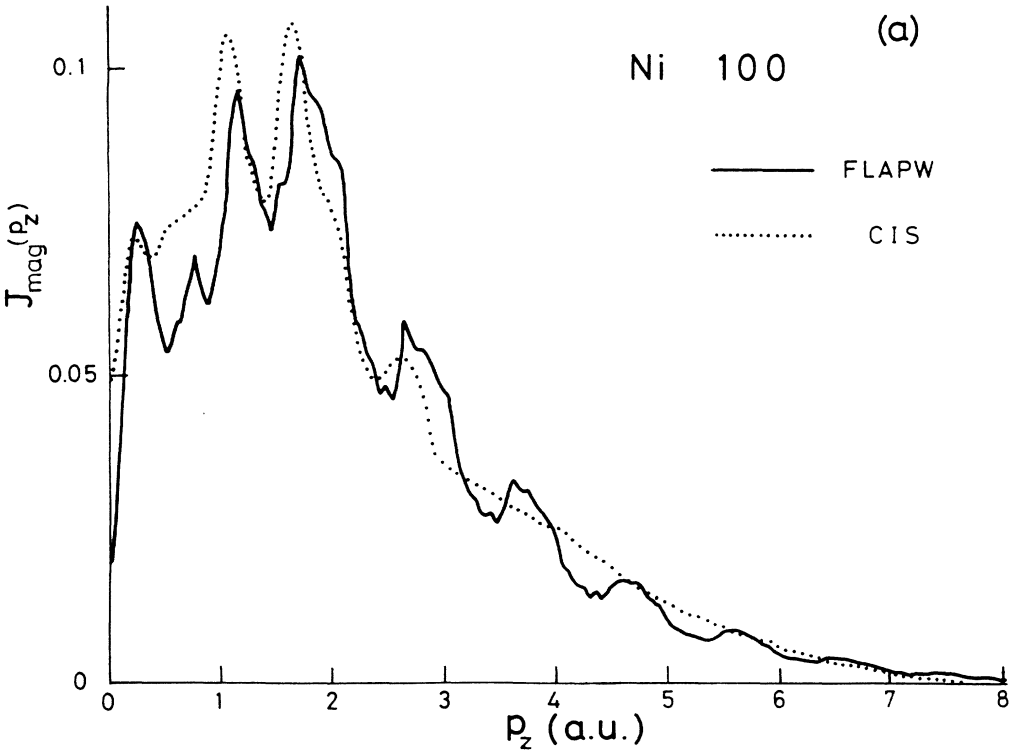

FIG. 9. Theoretical magnetic Compton profiles of nickel for (a) ⟨100⟩, (b) ⟨110⟩, and (c) ⟨111⟩ directions. The FLAPW calculations are denoted by FLAPW, and CIS represents the combined interpolation scheme calculations (Ref. 34).

scales of the $J_{mag}(p_z)$'s shown in Ref. 13 are arbitrary, the direct comparison between their results and ours is not possible. However, in the comparison between the normalized results to the experiment by Sakai *et al.*,[16] the KKR results are higher near $p_z=0$ a.u., especially in the ⟨100⟩ direction, and lower at $p_z>2$ a.u. than both the parametrized FLAPW and FLAPW ones, respectively. Generally, in the band calculations, the KKR and LMTO methods have disadvantages in the representation of the wave functions, compared with the APW and LAPW

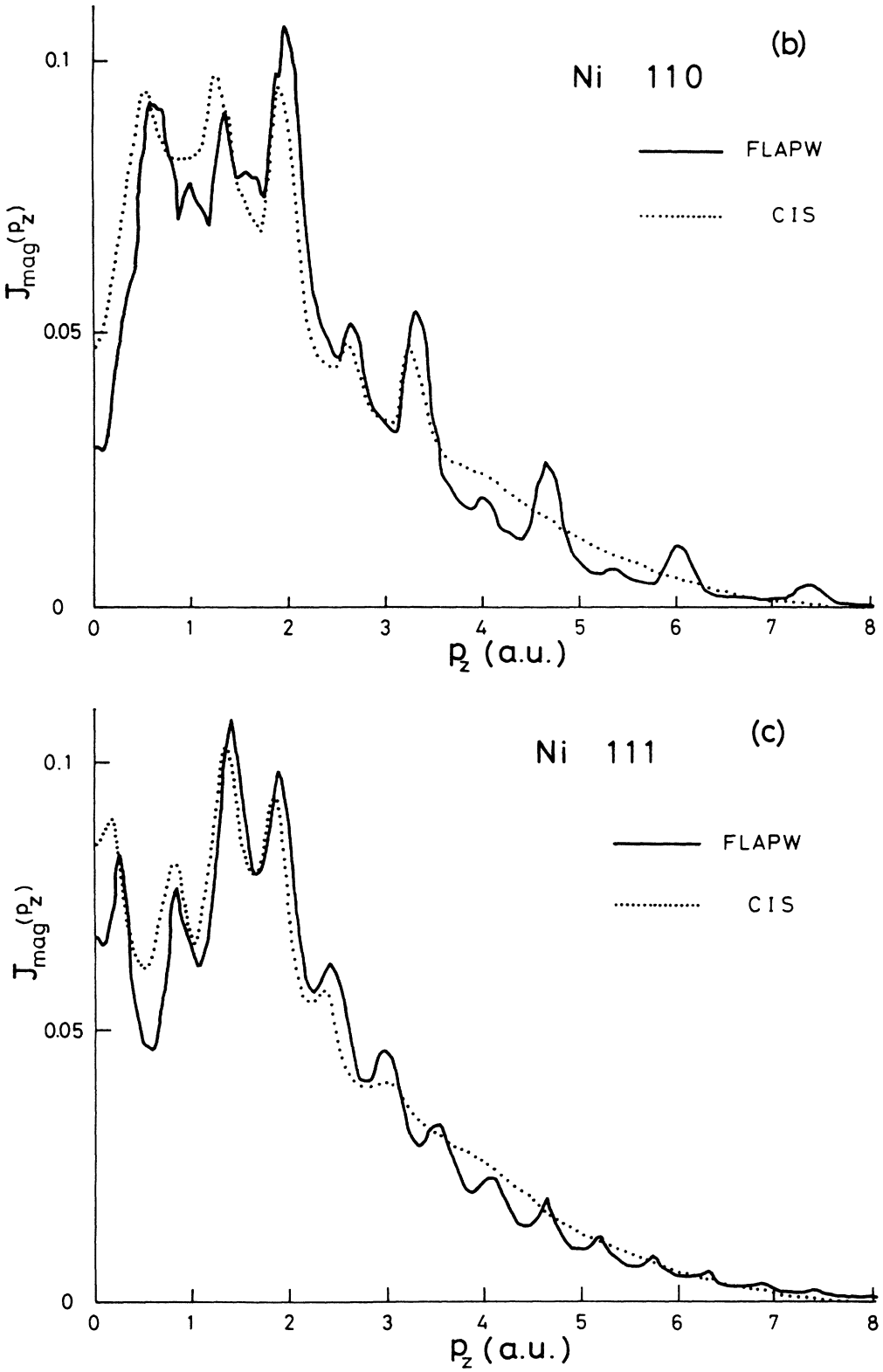

FIG. 9. (*Continued*).

methods, that is, the problem of the description of the wave function outside the inscribed sphere in the KKR method,[32] and the necessity of the correction of the overlapping sphere approximation in the LMTO method.[33] The differences between our results and the LMTO and KKR ones mentioned above will be mainly due to these disadvantages.

In the case of nickel, our FLAPW calculations are compared with the combined-interpolation-scheme (CIS) ones by Rennert *et al.*[34] In the CIS band-structure calculation of nickel, Rennert *et al.* have taken into account the information from the angle-resolved photoemission experiment by Eastman *et al.*[26] The CIS band structure corresponds to a magnetization of $0.56\mu_B$. The calculated $J_{\rm mag}(p_z)$'s by Rennert *et al.* are compared with our FLAPW results in Fig. 9. In the figure, the characteristic structures of the FLAPW results at $p_z<4$ a.u., shown in Sec. III A 2, are also observed in the CIS ones. However, the CIS calculations are higher near $p_z=0$ a.u. in all directions than the FLAPW ones. These differences may be attributed to an underestimation of the negative polarization of the s-p-like electrons in the CIS calculations by Rennert *et al.* This underestimation may be mainly due to the insufficient number of both four orthogonalized-plane-waves and 70 reciprocal-lattice vectors in their calculations.

V. CONCLUSIONS

It has been shown that the experimental $J_{\rm mag}(p_z)$'s of iron and nickel by Sakai *et al.*,[16] which have been measured with excellent statistical accuracy, are fairly well described by the FLAPW calculations based on the LSDA. In the case of iron, the parametrized FLAPW calculations, which have been performed by lowering the center of gravity of p states to reproduce correctly the N-centered hole pocket of the third minority-spin band, show an excellent agreement with the experimental data.[16] This indicates that some appropriate potential with nonlocal correction to the LSDA is needed to obtain a better description of the $J_{\rm mag}(p_z)$ of iron. It is indicated that the state-dependent potential used in the previous APW calculations[12] is inadequate to describe the $J_{\rm mag}(p_z)$'s of iron. In the case of nickel, the FLAPW calculations leave a slight but noticeable discrepancy in the $J_{\rm mag}(p_z)$ along the $\langle 100\rangle$ direction. This discrepancy seems to be attributed to nonlocal potential due to electron-electron correlations. However, in order to find a prescription to modify the potential based on the LSDA, spin-orbit interactions neglected in the present calculations should first be taken into account. Furthermore, it is desired to measure the $J_{\rm mag}(p_z)$ of nickel with higher statistical accuracy. Thus, the present studies have demonstrated that the investigation of the $J_{\rm mag}(p_z)$'s of iron and nickel is useful for evaluating the accuracy of the spin-dependent wave functions in the band calculations. More elaborate experiments with a high-momentum resolution will provide a further critical test of band theories.

ACKNOWLEDGMENTS

We sincerely acknowledge Dr. N. Sakai of Riken for his valuable discussions and sending of data of magnetic Compton profiles prior to publication. Financial support in part by the Grant-in-Aid for Scientific Research from the Ministry of Education, Science and Culture is acknowledged.

[1] S. Wakoh and J. Yamashita, J. Phys. Soc. Jpn. **21**, 1712 (1966).
[2] J. Callaway and C. S. Wang, Phys. Rev. B **16**, 2095 (1977).
[3] C. S. Wang and J. Callaway, Phys. Rev. B **15**, 298 (1977).
[4] V. L. Moruzzi, J. F. Janak, and A. R. Williams, *Calculated Electronic Properties of Metals* (Pergamon, New York, 1978).
[5] J. R. Anderson, D. A. Papaconstantopoulos, L. L. Boyer, and J. E. Schirber, Phys. Rev. B **20**, 3172 (1979).
[6] H. J. F. Jansen and F. M. Mueller, Phys. Rev. B **20**, 1426 (1979).
[7] L. Kleinman and F. Mednick, Phys. Rev. B **25**, 1090 (1982).
[8] F. Weling and J. Callaway, Phys. Rev. B **26**, 710 (1982).
[9] T. Nautiyal and S. Auluck, Phys. Rev. B **32**, 6424 (1985).
[10] N. Sakai and H. Sekizawa, Phys. Rev. B **36**, 2164 (1987).
[11] D. N. Timms, A. Brahmia, P. Collins, S. P. Collins, M. J. Cooper, R. S. Holt, P. P. Kane, G. Clark, and D. Laundy, J. Phys. F **18**, L57 (1988).
[12] S. Wakoh and Y. Kubo, J. Magn. Magn. Mater. **5**, 202 (1977).
[13] J. Poulter and J. B. Staunton, J. Phys. F **18**, 1877 (1988).
[14] M. J. Cooper, S. P. Collins, D. N. Timms, A. Brahmia, P. P. Kane, R. S. Holt, and D. Laundy, Nature **333**, 151 (1988); M. J. Cooper, Physica B **159**, 137 (1989).
[15] P. Genoud and A. K. Singh, J. Phys. Condens. Mat. **1**, 5363 (1989).
[16] N. Sakai, M. Ito, H. Kawata, T. Iwazumi, M. Ando, Y. Kubo, S. Asano, N. Shiotani, Y. Sakurai, and S. Nanao (unpublished).
[17] S. Yamamoto, H. Kawata, H. Kitamura, M. Ando. N. Sakai, and N. Shiotani, Phys. Rev. Lett. **62**, 2672 (1989).
[18] M. Weinert, E. Wimmer, and D. R. Hamann, Phys. Rev. B **25**, 1109 (1982).
[19] G. G. Lonzairch, in *Electrons at the Fermi Surface,* edited by M. Springford (Cambridge University Press, Cambridge, 1980).
[20] U. von Barth and L. Hedin, J. Phys. C **5**, 1629 (1972).
[21] D. D. Koelling and B. H. Harmon, J. Phys. C **10**, 3107 (1977).
[22] P. Genoud, A. K. Singh, A. A. Manuel, T. Jarlborg, E. Walker, M. Peter, and M. Weller, J. Phys. F **18**, 1933 (1988).
[23] A. M. Turner, A. W. Donoho, and J. L. Erskine, Phys. Rev. B **29**, 2986 (1984).
[24] H. Danan, A. Herr, and A. J. H. Meyer, J. Appl. Phys. **39**, 669 (1968).
[25] C. G. Shull and H. A. Mook, Phys. Rev. Lett. **16**, 184 (1966).
[26] D. E. Eastman, F. J. Himpsel, and J. A. Knapp, Phys. Rev. Lett. **40**, 1514 (1978).
[27] F. J. Himpsel, J. A. Knapp, and D. E. Eastman, Phys. Rev. B **19**, 2919 (1979).
[28] W. Eberhardt and E. W. Plummer, Phys. Rev. B **21**, 3245 (1980).
[29] L. C. Davis, J. Appl. Phys. **59**, R25 (1986).
[30] D. G. Kanhere and R. M. Singru, J. Phys. F **7**, 2603 (1977).
[31] R. V. Coleman, W. H. Lowrey, and J. A. Polor, Jr., Phys. Rev. B **23**, 2491 (1981).
[32] F. S. Ham and B. Segall, Phys. Rev. **124**, 1786 (1961).
[33] A. K. Singh and T. Jarlborg, J. Phys. F **15**, 727 (1985).
[34] P. Rennert, G. Carl, and W. Hergert, Phys. Status Solidi B **120**, 273 (1983).